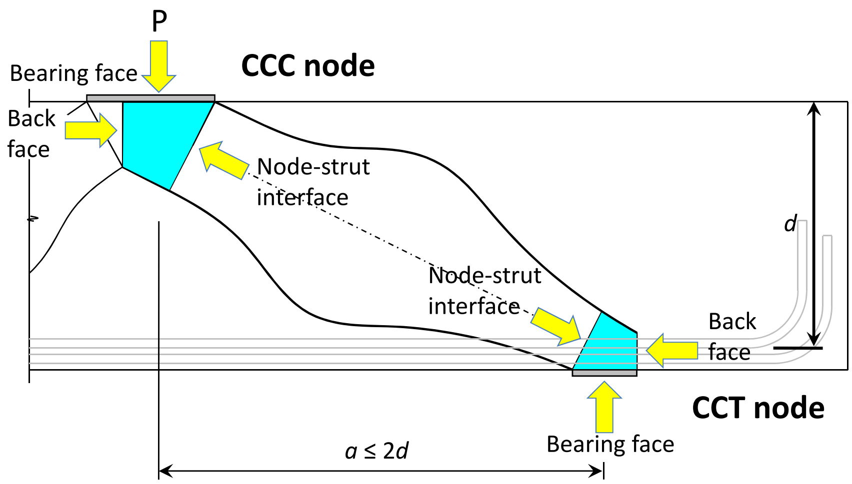

Figure 2 – Strut bounded by a CCC and CCT node at each end.

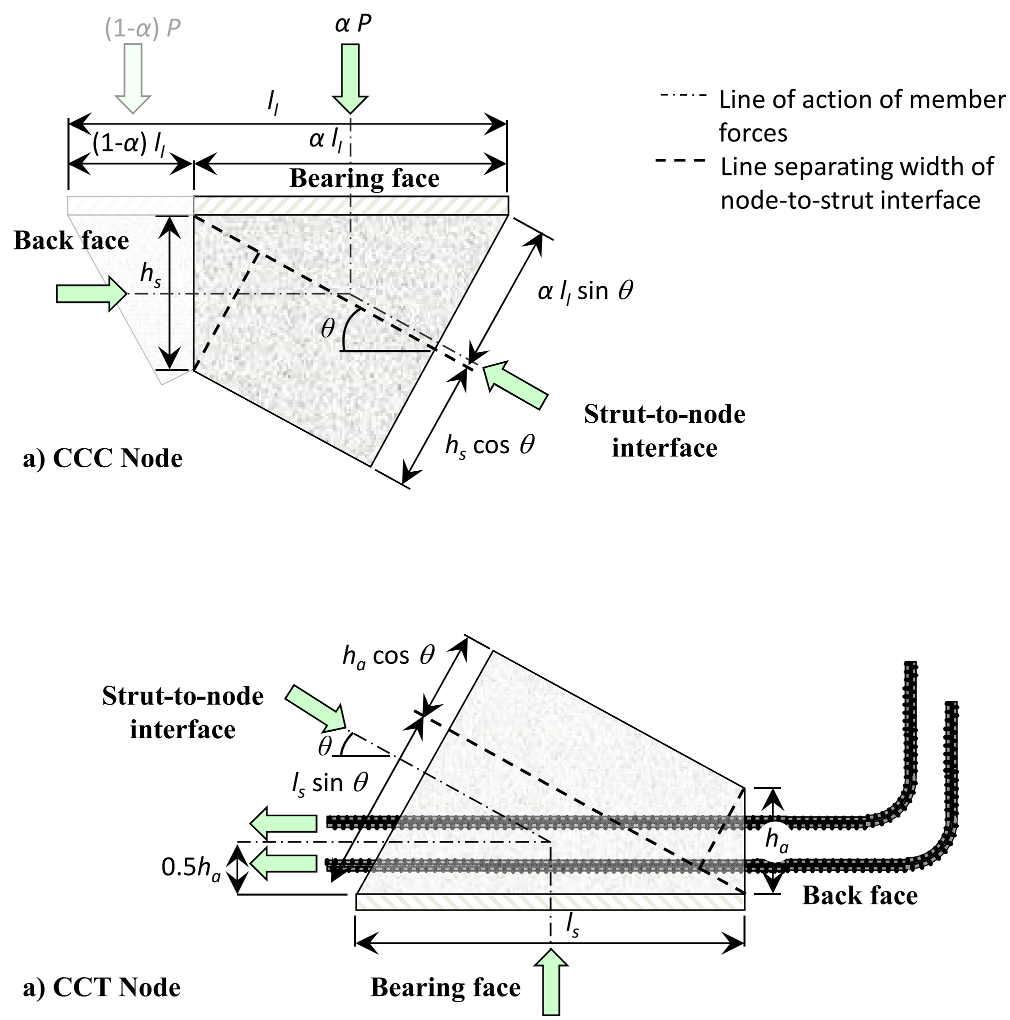

Figure 3 – Nodal proportions for a: a) CCC and b) CCT node.

Where,

h_a = height of the back face of a CCT node (taken as twice the distance from the near surface to the centroid of the tension reinforcement).

h_s = height of the back face of a CCC node (taken as the depth of the rectangular stress block defined in ACI 318).

l_l = length of the bearing plate at the CCC node.

l_s = length of the bearing plate at the CCT node.

α = fraction of the applied load that is resisted by the near support.

θ = angle of the strut axis with respect to the horizontal axis.

After the nodal geometries have been defined, stresses applied to the node face must be compared with the effective compressive strength in order to ensure that concrete does not crush. Stress in the steel reinforcement is compared to the yield strength. For the member shown in Figure 2, this results in the following seven stress checks: back face of the CCC and CCT node; bearing face of the CCC and CCT node; node-to-strut interface at the CCC and CCT node; and stress in the longitudinal steel reinforcement. Checking stresses at these locations accounts for all possible failure modes of a deep beam with two detailing exceptions. Proper anchorage of the tie must be provided in order to ensure that the tie can achieve its design capacity. Also, minimum web reinforcement is required in order to ensure that the member has the ability to redistribute stresses and prevent splitting failure of the strut.

After checking stresses at critical locations, the governing value determines the capacity of the structure. Table 1 lists the strengths stipulated within the ACI 318-11 STM provisions.

Table 1 –Strength of Strut and Tie Modeling Elements per ACI 318-11

Element	Design Check	Effective Compressive Strength	Strength Reduction Factor, ϕ
CCC Node	Bearing	$0.85 \cdot (1.0) \cdot f_c' =$ $\mathbf{0.85\, f_c'}$	0.75
	Back Face	$0.85 \cdot (1.0) \cdot f_c' =$ $\mathbf{0.85\, f_c'}$	
	Node-to-Strut Interface	$0.85 \cdot (0.75) \cdot f_c' =$ $\mathbf{0.64\, f_c'}$	
CCT Node	Bearing	$0.85 \cdot (0.80) \cdot f_c' =$ $\mathbf{0.68\, f_c'}$	
	Back Face	$0.85 \cdot (0.80) \cdot f_c' =$ $\mathbf{0.68\, f_c'}$	
	Node-to-Strut Interface	$0.85 \cdot (0.75) \cdot f_c' =$ $\mathbf{0.64\, f_c'}$	
Element	**Design Check**	**Tensile Strength**	
Tie	Tie	f_y	

EXPERIMENTAL INVESTIGATION

To accomplish the objectives of this research project, it was necessary to develop an experimental program. Previously reported data in the literature was insufficient with regard to the objectives of this research project for two reasons. First, only a limited amount of information related to the serviceability of deep beams (such as the diagonal crack widths at various stages of the loading) was identified in the literature. Second, the cross-sectional dimensions of the previously tested deep beams, particularly the widths, were found to be drastically smaller than structural members designed in practice. In an effort to eliminate scaling effects, it was determined that testing large-scale specimens provided the best means to improve the design and performance of in-service structural members of comparable size.

In order to illustrate the scale of previously tested deep beam specimens, Figure 4 includes a comparison between several bent caps in Texas, specimens tested as part of past research programs, and specimens tested as part of the study[1] presented in this paper. Upon comparison, it is clear that the scale of actual bent caps in service is significantly different than that of the deep beam specimens tested as part of past research programs.

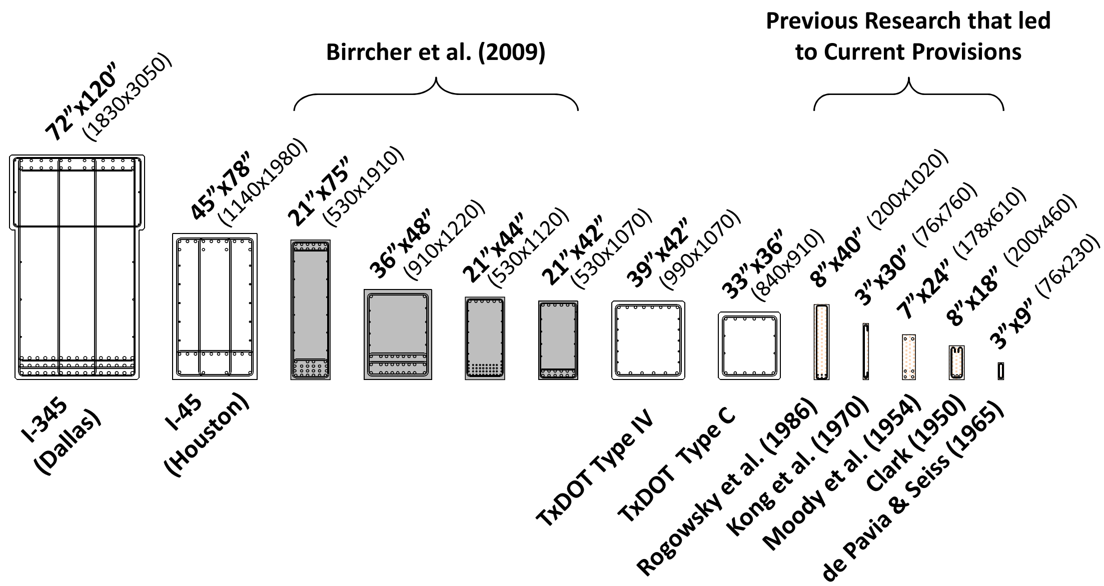

Figure 4 – Scaled comparison of actual bent caps in service and deep beams tested as part of previous research studies (dimensions shown in parentheses are in mm).

In order to isolate the primary objectives of the study presented in this paper, the authors developed an experimental program that included five separate testing series. The experimental variables in these testing series included: i) the distribution of stirrups across the web; ii) the width and length of the load and support plates; iii) the quantity of web reinforcement; and iv) the member depth. In all, thirty-seven (37) deep beam tests were conducted as part of this study. These tests represent some of the largest deep beam specimens tested and a significant contribution to the literature. Complete details of these 37 specimens are presented elsewhere[1]. Vital details for these 37 specimens are given in Table 2.

Table 2 – Birrcher et al.[1] Beam Details

Test I.D.	b_w in.	h in.	d in.	ρ_l	ρ_l'	ρ_v	s_v in	ρ_h	s_h in.	Sprt Plate in.	Load Plate in.	a/d ratio
I-03-2	21	44	38.5	0.0229	0.0116	0.0029	6.5	0.0033	5.75	16x21	20x21	1.84
I-03-4	21	44	38.5	0.0229	0.0116	0.0030	7.0	0.0033	5.75	16x21	20x21	1.84
I-02-2	21	44	38.5	0.0229	0.0116	0.0020	9.5	0.0020	9.5	16x21	20x21	1.84
I-02-4	21	44	38.5	0.0229	0.0116	0.0021	10.0	0.0020	9.5	16x21	20x21	1.84
II-03-CCC2021	21	42	38.6	0.0231	0.0115	0.0031	9.5	0.0045	6.6	10x21	20x21	1.84
II-03-CCC1007	21	42	38.6	0.0231	0.0115	0.0031	9.5	0.0045	6.6	10x21	10x7	1.84
II-03-CCT1021	21	42	38.6	0.0231	0.0115	0.0031	9.5	0.0045	6.6	10x21	36x21	1.84
II-03-CCT0507	21	42	38.6	0.0231	0.0115	0.0031	9.5	0.0045	6.6	5x7	36x21	1.84
II-02-CCT0507	21	42	38.6	0.0231	0.0115	0.0020	15.0	0.0019	10	5x7	36x21	1.84
II-02-CCC1007	21	42	38.6	0.0231	0.0115	0.0020	15.0	0.0019	10.1	10x21	10x7	1.84
II-02-CCC1021	21	42	38.6	0.0231	0.0115	0.0020	15.0	0.0019	10.1	10x21	10x21	1.84
II-02-CCT0521	21	42	38.6	0.0231	0.0115	0.0020	15.0	0.0019	10.1	5x21	20x21	1.84
III-1.85-00	21	42	38.6	0.0231	0.0115	0.000	-	0.000	-	16x21	20x21	1.84
III-2.5-00	21	42	38.6	0.0231	0.0115	0.000	-	0.000	-	16x21	20x21	2.47
III-1.85-02	21	42	38.6	0.0231	0.0115	0.0020	14.5	0.0019	10.1	16x21	20x21	1.84
III-1.85-025	21	42	38.6	0.0231	0.0115	0.0024	12.0	0.0014	7.6	16x21	20x21	1.84
III-1.85-03	21	42	38.6	0.0231	0.0115	0.0029	10.0	0.0029	10.1	16x21	20x21	1.84
III-1.85-01	21	42	38.6	0.0231	0.0115	0.0010	18.0	0.0014	7.6	16x21	20x21	1.84
III-1.85-03b	21	42	38.6	0.0231	0.0115	0.0031	6.0	0.0029	10.1	16x21	20x21	1.84
III-1.85-02b	21	42	38.6	0.0231	0.0115	0.002	9.5	0.0019	10.1	16x21	20x21	1.84
III-1.2-02	21	42	38.6	0.0231	0.0115	0.002	9.5	0.0019	10.1	16x21	20x21	1.20
III-1.2-03	21	42	38.6	0.0231	0.0115	0.0031	9.5	0.0029	10.1	16x21	20x21	1.20
III-2.5-02	21	42	38.6	0.0231	0.0115	0.002	9.5	0.0019	10.1	16x21	20x21	2.49
III-2.5-03	21	42	38.6	0.0231	0.0115	0.0031	9.5	0.0029	10.1	16x21	20x21	2.49
IV-2175-1.85-02	21	75	68.9	0.0237	0.0129	0.0021	9.5	0.0019	10.1	16x21	29x21	1.85
IV-2175-1.85-03	21	75	68.9	0.0237	0.0129	0.0031	9.5	0.0029	10.1	16x21	29x21	1.85
IV-2175-2.5-02	21	75	68.9	0.0237	0.0129	0.0021	14.25	0.0021	14.25	16x21	24x21	2.50
IV-2175-1.2-02	21	75	68.9	0.0237	0.0129	0.0021	14.25	0.0021	14.25	16x21	24x21	1.20
IV-2123-1.85-03	21	23	19.5	0.0232	0.0116	0.0030	6.25	0.0030	6.25	16x21	16.5x21	1.85
IV-2123-1.85-02	21	23	19.5	0.0232	0.0116	0.0020	5.25	0.0017	6.25	16x21	16.5x21	1.85
IV-2123-2.5-02	21	23	19.5	0.0232	0.0116	0.0020	5.25	0.0017	6.25	16x21	15.5x21	2.50
IV-2123-1.2-02	21	23	19.5	0.0232	0.0116	0.0020	5.25	0.0017	6.25	16x21	18x21	1.20
M-03-4-CCC2436	36	48	40	0.0293	0.0043	0.0031	11	0.0027	6.5	16x36	24x26	1.85
M-03-4-CCC0812	36	48	40	0.0293	0.0043	0.0031	11	0.0027	6.5	16x36	8x12	1.85
M-09-4-CCC2436	36	48	40	0.0293	0.0043	0.0086	4	0.0027	6.5	16x36	24x36	1.85
M-02-4-CCC2436	36	48	40	0.0293	0.0043	0.0022	10	0.0022	8	16x36	24x36	1.85
M-03-2-CCC2436	36	48	40	0.0293	0.0022	0.0031	11	0.0027	6.5	16x36	24x36	1.85

Note: Table 2M in Appendix presents the above table with units converted to S.I. equivalent
1 in. = 25.4 mm.

b_w = beam width
h = beam height
d = distance form extreme compression fiber to centroid of tensile reinforcement
ρ_l = ratio of longitudinal tensile reinforcement to effective area *(A_s / $b_w d$)*
ρ_l' = ratio of longitudinal compression reinforcement to effective area *(A'_s / $b_w d$)*
ρ_v = ratio of vertical web reinforcement to effective area *(A_v / $b_w s_v$)*
s_v = spacing of vertical web reinforcement
ρ_h = ratio of horizontal web reinforcement to effective area *(A_h / $b_w s_h$)*
s_h = spacing of horizontal web reinforcement
Load Plate = dimensions of the load bearing plate measured in the longitudinal and transverse direction of the beam (*l* x *w*)
Sprt Plate = dimensions of the support bearing plate measured in the longitudinal and transverse direction of the beam (*l* x *w*)

A testing frame was designed for an upside-down simply supported beam test. The load was applied via a 6,000 kip (26,700 kN) capacity, double-acting hydraulic ram. 500-kip (2,200 kN) capacity load cells measured the reaction at each rod location. Therefore, it was possible to directly measure the total reaction at each support. Beams were loaded monotonically in approximately 30 to 50 kip (130 to 220 kN) increments. Also, two tests were conducted on each beam. First, the beam was loaded near one support corresponding to the appropriate a/d ratio. After a shear failure occurred in the test region under investigation, external clamps were installed to strengthen the failed portion. The actuator was moved to the opposite end of the beam and positioned based on the appropriate a/d ratio. The beam was loaded again, and the behavior of the second test region was monitored. Complete details with regard to the test setup and testing procedures are available elsewhere[1]. A typical test in progress is illustrated in Figure 5.

Figure 5 – Testing in progress for a 21 x 42 in. (530 x 1070 mm) deep beam specimen.

RESULTS

The experimental results for the 37 tests conducted by Birrcher et al. [1] are presented in Table 3. Other important details of these specimens are provided elsewhere[1].

Table 3 – Birrcher et al.[1] Experimental Results

Test I.D.	b_w in.	d in.	f_c' psi	f_{yl} ksi	f_{yv} ksi	a/d ratio	V_{crack} kip	$\frac{V_{crack}}{\sqrt{f'_c} \cdot b_w d}$	V_{test} kip	$\frac{V_{test}}{f'_c \cdot b_w d}$	$\frac{V_{test}}{\sqrt{f'_c} \cdot b_w d}$
I-03-2	21	38.5	5240	73	67	1.84	144	2.5	569	0.13	9.7
I-03-4	21	38.5	5330	73	73	1.84	-	-	657	0.15	11.1
I-02-2	21	38.5	3950	73	67	1.84	121	2.4	454	0.14	8.9
I-02-4	21	38.5	4160	73	73	1.84	-	-	528	0.16	10.1
II-03-CCC2021	21	38.6	3290	64	65	1.84	139	3.0	500	0.19	10.7
II-03-CCC1007	21	38.6	3480	64	65	1.84	-	-	477	0.17	10.0
II-03-CCT1021	21	38.6	4210	66	71	1.84	-	-	635	0.19	12.1
II-03-CCT0507	21	38.6	4410	66	71	1.84	146	2.7	597	0.17	11.1
II-02-CCT0507	21	38.6	3120	69	64	1.84	94	2.1	401	0.16	8.9
II-02-CCC1007	21	38.6	3140	69	64	1.84	-	-	335	0.13	7.4
II-02-CCC1021	21	38.6	4620	69	67	1.84	132	2.4	329	0.09	6.0
II-02-CCT0521	21	38.6	4740	69	67	1.84	-	-	567	0.15	10.2
III-1.85-00	21	38.6	3170	66	-	1.84	98	2.1	365	0.14	8.0
III-2.5-00	21	38.6	3200	66	-	2.47	-	-	82	0.03	1.8
III-1.85-02	21	38.6	4100	69	64	1.84	112	2.2	488	0.15	9.4
III-1.85-025	21	38.6	4100	69	64	1.84	-	-	516	0.16	9.9
III-1.85-03	21	38.6	4990	69	64	1.84	137	2.4	412	0.10	7.2
III-1.85-01	21	38.6	5010	69	63	1.84	-	-	273	0.07	4.8
III-1.85-03b	21	38.6	3300	69	62	1.84	114	2.4	471	0.18	10.1
III-1.85-02b	21	38.6	3300	69	62	1.84	-	-	468	0.17	10.1
III-1.2-02	21	38.6	4100	66	60	1.20	165	3.2	846	0.25	16.3
III-1.2-03	21	38.6	4220	66	68	1.20	-	-	829	0.24	15.7
III-2.5-02	21	38.6	4630	66	62	2.49	105	1.9	298	0.08	5.4
III-2.5-03	21	38.6	5030	66	65	2.49	-	-	516	0.13	9.0
IV-2175-1.85-02	21	68.9	4930	68	66	1.85	216	2.1	763	0.11	7.5
IV-2175-1.85-03	21	68.9	4930	68	66	1.85	218	2.1	842	0.12	8.3
IV-2175-2.5-02	21	68.9	5010	68	64	2.50	144	1.4	510	0.07	5.0
IV-2175-1.2-02	21	68.9	5010	68	64	1.20	262	2.6	1223	0.17	11.9
IV-2123-1.85-03	21	19.5	4160	66	66	1.85	60	2.3	329	0.19	12.5
IV-2123-1.85-02	21	19.5	4220	66	81	1.85	65	2.4	347	0.20	13.0
IV-2123-2.5-02	21	19.5	4570	65	58	2.50	51	1.8	161	0.09	5.8
IV-2123-1.2-02	21	19.5	4630	65	58	1.20	124	4.5	592(f)	0.31	21.2
M-03-4-CCC2436	36	40	4100	67	61	1.85	354	3.8	1128	0.19	12.2
M-03-4-CCC0812	36	40	3000	65	63	1.85	-	-	930	0.22	11.8
M-09-4-CCC2436	36	40	4100	67	61	1.85	-	-	1415(f)	0.24	15.3
M-02-4-CCC2436	36	40	2800	65	63	1.85	256	3.4	1102	0.27	14.5
M-03-2-CCC2436	36	40	4900	68	62	1.85	-	-	1096(i)	0.16	10.9

Note: Table 3M in Appendix presents the above table with units converted to S.I. equivalent
1 in. = 25.4 mm; 1 kip = 4.45 kN; 1 MPa = 145 psi
(f): Maximum shear carried in specimen upon the occurrence of concrete crushing at the compression face.
(i): Test was stopped due to initiation of yielding of the tensile reinforcement and crushing of concrete at the compression face.

b_w = beam width
d = distance from extreme compression fiber to centroid of tensile reinforcement.
f_c' = compressive strength of concrete at the time of testing measured in accordance with ASTM C39.
f_{yl} = yield strength of longitudinal reinforcement measured in accordance with ASTM A370.
f_{yv} = yield strength of vertical web reinforcement measured in accordance with ASTM A370.
f_{yh} = yield strength of horizontal web reinforcement measured in accordance with ASTM A370.
***a/d* ratio** = shear span-to-depth ratio
V_{crack} = shear carried in the test region when the first diagonal crack formed.
V_{test} = maximum shear carried in middle of the test region, including the estimated self-weight of the specimen and transfer girder.

DEEP BEAM DATABASE

In order to evaluate ACI 318-11 STM provisions, a database containing 868 deep beam shear tests (a/d ≤ 2.5) was collected from the literature. The aforementioned 37 tests were added to the database resulting in a total of 905 tests; referred to as the "collection database". Test results were removed if they lacked adequate details to perform an STM analysis or if the specimen details were not representative of actual members designed in practice. The resulting database is referred to as the "evaluation database". An overview of the filtering process is presented in Table 4. Additional details and justification of the filtering process is presented elsewhere[1]. Characteristics of the specimens in the evaluation database are illustrated in Figure 6.

Table 4 – Filtering of Deep Beam Database

		No. Tests
Collection Database		**905**
Filtering Criteria	Incomplete plate size info.	-284
	Subjected to uniform loading	-7
	Stub column failure	-3
	$f_c' < 2000$ psi (13.8 MPa)	-4
	$b_w < 4.5$ in. (114 mm)	-222
	$b_w \cdot d < 100$ in^2 (645 cm2)	-73
	$d < 12$ in. (300 mm)	-13
	$\Sigma\rho_\perp < 0.001$	-120
Evaluation Database		**179**

Note: $\boldsymbol{\rho_\perp}$: ratio of transverse perpendicular to the strut axis as defined by ACI 318-11, equation A-4.

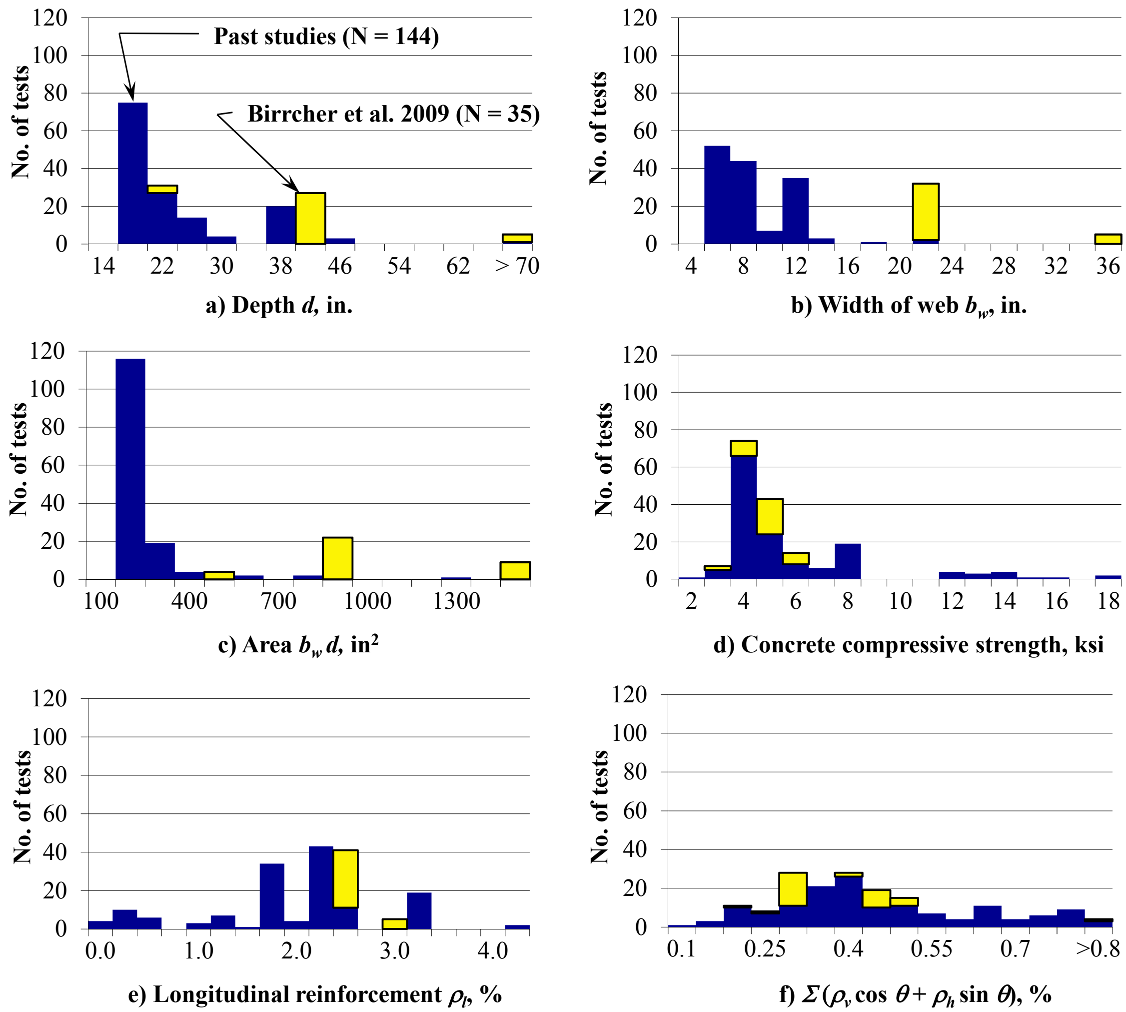

Figure 6 – Comparison of beam characteristics between Birrcher et al. (2009) and past research studies within the Evaluation Database. (1 in. = 25.4 mm; 1 MPa = 145 psi)

EVALUATION OF ACI 318 STM PROVISIONS

Based on the truss model illustrated in Figure 2, the performance of the ACI 318-11 STM provisions is measured using the 179 deep beam shear tests in the evaluation database. The ratio of experimental to calculated capacity was determined for all of the beams; a value greater than one indicates a conservative estimation of strength. Results are presented in Table 5.

Table 5 – Calculated Capacity of Deep Beam Specimens per ACI 318-11 STM Provisions

No. Tests = 179	$\frac{\text{Experimental}}{\text{Calculated}}$
Min. =	0.87
Max. =	9.80
Mean =	1.80
No. Unconservative =	3
COV =	0.58

A primary goal of this research study was to improve the ACI 318-11 STM design procedure. According to MacGregor[7], a 'design procedure' should satisfy the following four criteria: i) simplicity in application; ii) compatibility with tests of D-regions; iii) compatibility with other sections of the code; and iv) compatibility with other codes. In keeping with these considerations, the authors developed recommendations to improve the ACI 318-11 STM procedures. These recommendations are in large part consistent with the current ACI 318-11 STM provisions but also contain key components from other design provisions[8-9]. Birrcher et al.[1] presented a comprehensive derivation of these recommendations. As such, the authors recommend adoption of the following strut and tie modeling provisions.

The effective compressive strength of all faces of a node may be increased when triaxial confinement is present. Increasing the capacity of all triaxially confined nodal faces improves the accuracy of a STM prediction without diminishing its conservatism. Tuchscherer et al.[2] substantiated this recommendation in detail. In order to maintain consistency with ACI 318-11, the effective capacity of concrete may be increased by a confinement factor of $\sqrt{A_2/A_1} \leq 2$ for all faces of a triaxially confined nodal region. The implications of this recommendation are examined within the evaluation database. The capacity of the nodal regions for all beams in the database is increased by the confinement factor and the ratio of experimental to calculated capacity is determined Results of this analysis are compared with the results that were previously calculated per ACI 318-11 (Table 5). A summary is presented in Figure 7.

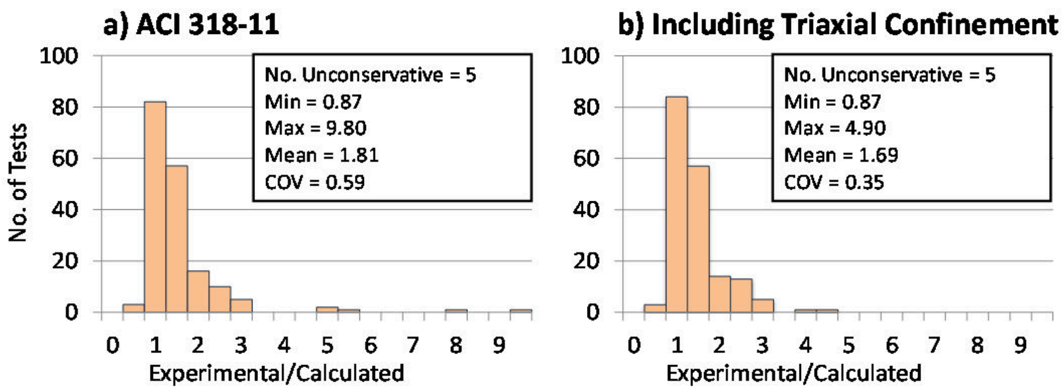

Figure 7 – Calculated capacity of deep beam specimens per: a) ACI 318-11; and b) including triaxial confinement.

As can be seen, applying the confinement factor to the beams in the database results in a more accurate estimate of strength (COV of 0.35 versus 0.59); and the number of beams whose capacity is unconservatively estimated (5) remains unchanged.

Stress applied to the back face of a CCT node is not critical when tie reinforcement is adequately developed. If tie forces are resisted by adequately developed reinforcement, then it is unlikely that crushing of concrete at the back face of a CCT node will occur. The authors[1] and previous researchers[10-11] have reached similar conclusions. Also this philosophy is consistent with the recommendations of the International Federation of Structural Concrete (*fib*)[9].

The evaluation database was used to examine the criticality of stress applied to the back face of the CCT node. To this end, the following actions were taken: i) the capacity of all of the beams in the database was calculated according to the ACI 318-11 STM provisions; ii) the critical node face that controlled the beam capacity was noted; and iii) the capacity of each beam was then recalculated without consideration of the stress at the back face of the CCT node. As illustrated in Figure 8 prior to elimination of the stress check at the back face of CCT nodes, this particular stress check controlled the STM capacity calculated for 43% of all specimens included in the database. As shown in Figure 9, the elimination of stress check at the back face of a CCT node did not have a significant effect on the conservativeness or accuracy of STM calculations. In addition to these observations, it is essential to appreciate the fact that distress at the back face of CCT nodes was not reported for any of the 179 tests included in the evaluation database. As a result, the utility of performing stress checks under a "conventionally assumed" concentrated force at the back face of the CCT nodes is unsubstantiated – provided the reinforcement is sufficiently developed.

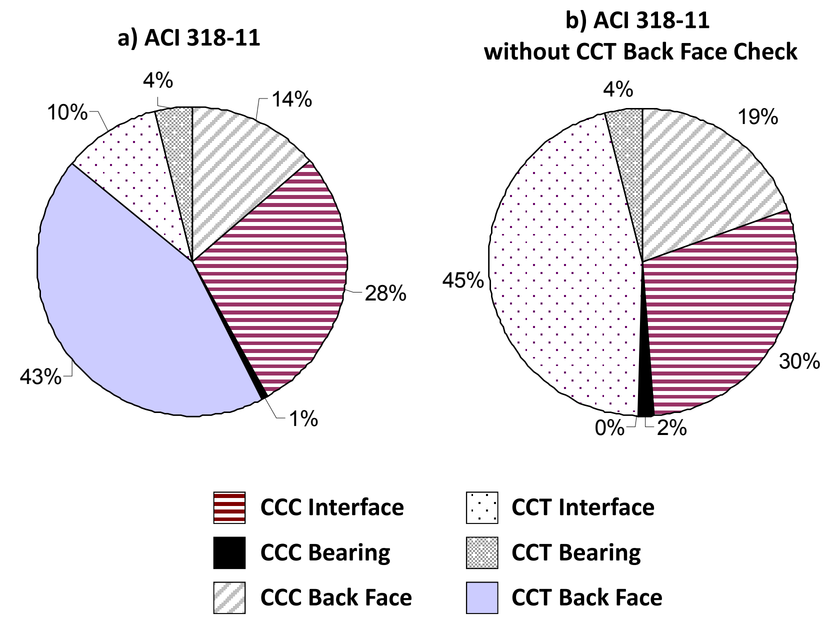

Figure 8 – Node interface that controls design capacity for all beams in the evaluation database.

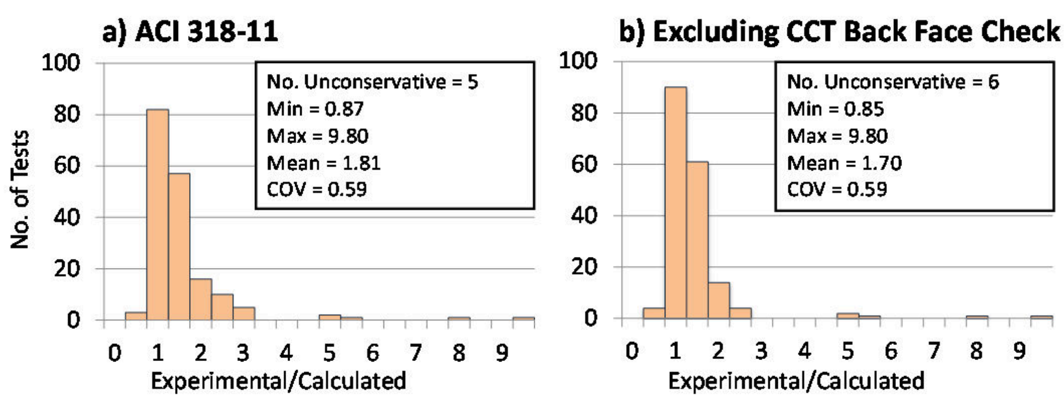

Figure 9 – Calculated capacity of deep beam specimens per ACI 318-11 with and without consideration of stresses at the back face of the CCT node.

As the compressive strength of concrete increases, the effective compressive strength at the strut to node interface shall increase at a diminishing rate. As the compressive strength of concrete increases, its shear strength increases at a rate that is less than proportional to the increase in compressive strength. High-strength concrete is typically considered that which has a compressive strength greater than 8000 psi (55 MPa). The cement paste of high-strength concrete is stronger than the aggregate and the quality of aggregate greatly contributes to its compressive strength. When a shear crack forms in a high-strength concrete member, it passes through the aggregate rather than following a path around it. As a result, shear cracks forming in high strength concrete are "smoother" and there is a corresponding reduction in the ability of the beam to transfer aggregate interlock forces at a shear crack. Previous researchers[12-15] have similarly noted that an increase in the compressive